Materials Today Bio 8 (2020) 100072

Contents lists available at ScienceDirect

Materials Today Bio

journal homepage: www.journals.elsevier.com/materials-today-bio

Blood-brain barrier amenable gold nanoparticles biofabrication in aged cell culture medium

F.U. Rehman [a,*,d], J. Bao [b,d], P. Muhammad [a,d], W. He [a], S. Hanif [a], M.A. Rauf [c]

[a] International Joint Centre for Biomedical Innovations, School of Life Sciences, Henan University, Jin Ming Avenue, Kaifeng, Henan, 475004, China
[b] State Key Lab of Bioelectronics, Southeast University, Sipailou 2, Nanjing, 210096, China
[c] Barbara Ann Karmanos Cancer Institute, Wayne State University Detroit, Michigan, USA

ARTICLE INFO

Keywords:
Cell culture medium
Blood-brain barrier
Gold nanoparticles
Green biosynthesis
Transferrin
Cell proteins

ABSTRACT

Green fabrication of nanoscale materials is highly desirable because of associated adverse effects with conventional nanomaterial biomedical applications. Moreover, the higher selective nature of the blood-brain barrier (BBB) limits the brain ailments treatment through conventional chemotherapy, thus providing room for nanotechnology-based modalities for BBB traversing. In this contribution, we have biosynthesized gold nanoparticles from the $HAuCl_4$ solution in the aged cells culture medium. This approach is highly facile without any other chemical utilization. The cell culture medium age and cell number can tune the Au nanoparticles (AuNPs) size from 2 to several hundred nm. The 24 h MTT assay and cell uptake studies *in vitro* and murine models' vital organs (liver, kidney, spleen, lung, and heart) study up to 48 h demonstrated that biosynthesized AuNPs were biocompatible and BBB amenable. Interestingly, the transferrin and cell culture medium isolated proteins were found factors responsible for $HAuCl_4$ solution biomineralization and size control. Moreover, the protein corona on biosynthesized AuNPs could help them traverse BBB both *in vitro* and *in vivo*, suggesting their potential applications for brain disease theranostics. In conclusion, the biosynthesis of AuNPs from aged cells medium is highly facile, green, and biocompatible for brain disease theranostics.

1. Introduction

The exponential increase in nanoscale materials biomedical applications has provided us with a new scaffold for daunting diseases theranostics [1–3]. However, the associated adverse effects because of the employment of hazardous chemicals during the fabrication process have limited their clinical applications. Therefore, new fabrication modalities are highly desired that could provide robust, hypoimmunogenic, biocompatible, and efficient nanoscale materials for biomedical applications [4]. The biosynthesis of nanomaterials by exploiting the potential of living sources viz plant [5], bacteria [6], fungi [7], and mammalian cells [8] has got a reputation in the recent past. These approaches are highly biocompatible and green with equal efficiency as that of conventional chemosynthesized nanomaterials.

The employment of a mammalian scaffold for the biosynthesis of nanoscale materials is relatively new and recently got popularity [9]. The mammalian scaffold utilizes biomolecules that are already present within living cells to biomineralize the administered salts to nanoscale materials. Recently, the biosynthesized nanoscale materials biomedical applications have been reported in several types of cancer and Alzheimer's disease [10]. So far, the iron [11], zinc [12], silver [13], iridium [14], and gold [11] nanoparticles have been biosynthesized and employed in cancer theranostics. It is well known that the cancer microenvironment is different from the healthy cells, having a higher number of reactive oxygen species (ROS), reduced and oxidized glutathione (GSH-GSSG), GAP(D)H, and lower pH value, providing an excellent scaffold for biomineralization of ionic salts to nanoscale materials [9]. Therefore, the biosynthesis is selectively orchestrated in the neoplastic environment that provides realm for selective targeting of tumors and helps in differentiation from healthy tissue.

We hypothesize that biomolecules present inside the cells may also be secreted into the surrounding microenvironment. Therefore, the cell culture media (i.e. making culture cells microenvironment) may provide the same scaffold for the nanomaterial's biosynthesis with higher biocompatibility for biomedical applications. Notably, cell proteins, especially the transferrin is essential for reduction and transportation

* Corresponding author.
E-mail address: dawarvet@hotmail.com (F.U. Rehman).
[d] These authors contributed equally.

https://doi.org/10.1016/j.mtbio.2020.100072
Received 20 May 2020; Received in revised form 15 July 2020; Accepted 21 July 2020
Available online 7 August 2020

agent for Fe^{+2} ions [15], have a crucial role in providing the reducing realm for other ionic salts reduction, including $HAuCl_4$ solution, where the $Au^{(+3)}$ is reduced to $Au^{(0)}$, thus forming AuNPs [16]. The nanoscale gold applications are well known in various diseases theranostics, including cancer [17]. To date, all reported biosynthetic mammalian cell-based modalities only provide evidence of intracellular nanoparticles formation. The intracellular nanoparticles/clusters formation has limited biomedical applications for certain diseases. Therefore, broad biomedical applications of mammalian biosynthesized nanoparticles are still a challenge.

In brain disease theranostics, the BBB role is very critical because of its selective amenability to a limited number of drugs, resulting in 98% of conventional medications fail to cross the BBB [18]. The BBB maintains homeostasis of the brain by only allowing small molecules, i.e. size <400 Da or having less than nine hydrogen binding, O_2, CO_2, alcohol, or glucose, whereas highly charged and large size molecules that may pose a threat to brain physiology are refrained [19]. Therefore, the nanotechnology may provide opportunities to overcome the BBB selectivity for therapeutic agents and enhance the drug permeation to cerebral milieu [20]. The nanoscale materials due to natural structural analogy to cell receptors/ligands are highly admired for BBB traversing [21–23].

Keeping in view these limitations, we have biosynthesized the AuNPs from the aged cell culture medium. The prolonged incubation time of the cultured cells results in a higher number of biomolecules secretion to cell culture media. Moreover, in contrast to previous reports, for the first-time, cell-free mammalian scaffold was employed to prepare the nanoscale materials, i.e. AuNPs.

2. Materials and methods

2.1. Chemical and instruments utilized

All chemicals used in this study were experimental grade and purchased from Sigma Aldrich, otherwise specified. The cell culture chemicals were purchased from HyClone Inc. USA. The UV–vis absorption and MTT optical density values were measured by SpectraMax® i3x, Molecular Devices, LLC. San Jose, CA. Malvern Zetasizer ZS measured the particle size and zeta potential. The cell's fluorescence imaging was performed by Zeiss LSM880 confocal microscope.

All animals used in the experiment were specific pathogen-free and provided with food and water ad libitum. A 12-h light on and off cycle within a full automatically controlled environment was provided. All the animals' experiments were performed under the guideline approved by Henan University Laboratory Animal Center and the Animal Care and use Committee of Henan University.

2.2. Procedure for cells culture

All the cell lines including U87 (glioblastoma), MCF-7 (breast cancer), MGC803 (gastric cancer), HeLa (cervical cancer), A549 (lung cancer), and healthy cells, i.e. L02 (hepatocytes) and RAW264.7 (macrophage) cells were purchased from the Chinese Academy of Sciences, Shanghai, China. The cells were cultured in Dulbecco's Modified Eagle Medium (DMEM) high glucose (HyClone™, Inc.) supplemented with 10% fetal bovine serum (FBS) and 1% penicillin-streptomycin solution, under standard incubation conditions of 37°C, 95% relative humidity and 5% CO2.

The monocytes were isolated from the bone marrow of BALB/C mice at the age of 4 weeks and 16–18 g weight, as per previously reported protocol [24]. After euthanasia, the long bones (femur, tibia, humerus, and radius) were isolated and washed with cold phosphate buffered saline (PBS) containing 2% FBS and 1 mM EDTA. Then bone marrow was isolated in the aseptic environment by flushing the bones with cold PBS at 4°C. Then cells were sieved with 70 μm filter and centrifuged to obtain the cells in a pellet form. Then, the supernatant was discarded, and the pellet was re-suspended in DMEM-F12 (Hyclone) medium supplemented with 10% FBS and 1% penicillin-streptomycin solution and macrophage colony stimulating factor (PROSPEC, protein specialists) and then incubated under standard conditions, i.e. 37°C, 95% RH, 5% CO_2. After 72 h, cell colonies were visible that were used for further experiments.

2.3. AuNPs biosynthesis

The glioblastoma (U87) cells were cultured in a standard medium, i.e. DMEM, high glucose containing 10% FBS, and 1% penicillin-streptomycin solution, under standard incubation conditions at 37°C, 5% CO_2, and 95% relative humidity. The media was collected after 24 h of aging. For a comparative study on other cell lines (i.e. HeLa, MCF-7, MGC08, RAW264.7, and monocytes), DMEM with 10% FBS was used as standard media. Then, it was centrifuged at 2000×*g* for 10 min and further centrifuged at 15,000×*g* for 30 min to ensure the removal of dead cells and debris. Then, the medium was mixed with 3.25 mM $HAuCl_4$ solution at the 1:1 ratio and incubated at 95°C with a shaking speed of 100 rpm for an hour. The color change was an indication of AuNPs formation that was further confirmed by dynamic light scattering (DLS) and transmission electron microscopy (TEM) etc.

2.4. AuNPs characterization

The morphology of the AuNPs was investigated by using high-resolution transmission electron microscope (HR-TEM) TEM, FEI Talos 200X, and JEOL USA Inc. Samples for HR-TEM analysis were prepared on carbon-coated copper grids. The films were allowed to dry before measurement. Elemental identification was performed using Thermo Scientific's Energy-dispersive X-ray fluorescence (EDXRF) operated at an accelerating voltage of 120 kV. X-ray photoelectron spectroscopy (XPS) experiments were performed on a ThermoFisher Scientific ESCALAB 250 spectrometer (XPS, Thermo ESCALAB 250). The surface chemical properties were investigated using a monochromatic Al Kα radiation source (h 1486.6 eV). The C1s, O 1s, and Au 4f core levels were recorded at pass energy of 29.35 eV and with a take-off angle of 90°.

2.5. Protein separation from cell culture media

The cell culture media after aging was isolated and collected in a 50 mL tube and then centrifuged at 2000×*g* for 20 min, followed by 15,000×*g* for 30 min at 4°C. Then, ultracentrifuge (Hitachi, N100) was used to isolate the proteins from cell culture media at 120,000×*g* for 90 min. The medium as the supernatant was used for downstream experiments.

2.6. MTT assay

Fibroblast cells were isolated from the mice by procedure reported earlier [25] and cultured in the 75 cm^2 culture flasks under standard incubation conditions. At 90% confluency, the cells were trypsinized (Trypsin 0.25%) and cultured in 96-well plate for 24 h. Then various concentrations (30, 60, 150, and 225 μM) of biosynthesized and chemosynthesized AuNPs were inoculated and further incubated for 24 h. Afterward, 10 μl of 5 mg/mL MTT solution was added to each well and further incubated for 4 h. The cell culture media was then discarded, and 200 μl of DMSO was added and vortexed for 10 min. The optical density value was recorded at 490 nm by using a microplate reader.

2.7. Cell uptake study

A total of 1.0×10^6 U87 cells were cultured in the special confocal Petri dishes for 24 h. Then 30 μM of biosynthesized and chemosynthesized AuNPs were inoculated and further incubated for 24 h. The cell nucleus was stained with DAPI for 5 min and then fixed with paraformaldehyde 4% solution for an additional 10 min. After washing three times with PBS, the cells were imaged under a confocal scanning laser microscope. (AuNPs were fluorescent at 488 nm excitation).

2.8. Trans-well BBB model preparation

The trans-well model was used to construct the *in vitro* BBB model by culturing the 1×10^6 bEnd.3 (endothelial) cells in the membranes (Millicell®) having a pore size of 100 nm. When the bEnd.3 cells confluence resistance became higher than 300 Ω (checked by EVOM2, world precision instruments, 175 Sarasota Center Blvd. Sarasota, FL 34240), the AuNPs were inoculated to the membrane having cultured bEnd.3 cells in the upper chamber and incubated for 24 h under standard incubation conditions and shear force. Meanwhile, 1×10^5 of the U87 cells were cultured on the round glass coverslips in a lower chamber of trans-well cell culture apparatus in 24 well plates. After 24 h, the U87 cells were incubated with DAPI solution (1:1000) for 5 min to stain the cell nucleus and then fixed with 4% paraformaldehyde solution for further 10 min. After 3 x washes with PBS, the coverslips were mounted on glass slides by using Thermofisher ProLong™ Gold Antifade Mountant. The U87 cells were then imaged under a confocal scanning microscope for AuNPs uptake at 488 nm, and cell nucleus at 358 excitations wavelength.

2.9. In vivo BBB crossing

A total number of 15 BALB/C female mice were randomly allocated to three groups named as biosynthesized, chemosynthesized, and control (PBS) group (n = 5). The age of mice was 6–8 weeks, with an average body weight of 18 ± 2 grams. They were injected with 100 μl of AuNPs (either chemosynthesized or biosynthesized) dissolved in PBS via the tail vein. At various time points of 01, 12, and 24 h, the mice were imaged under small animals *in vivo* bioimaging system (IVIS Lumina III, PerkinElmer). Moreover, the vital organs, including brain, were removed and also imaged for fluorescence intensity that represented the AuNPs accumulation in vital organs (excitation 488 nm, emission 670 nm). Later, the brain and vital organs were homogenized in 65% HNO_3 solution and evaluated for Au quantification under inductively coupled plasma (ICP) apparatus (PerkinElmer, Optima 8000 ICP-OES) by using an ICP standard protocol.

2.10. Histopathology for biocompatibility

A total of 12 ICR mice with a mean weight of 18 ± 2 g, and 6 weeks age were divided into two main groups, i.e. injected with chemosynthetic and biosynthetic AuNPs, which were further divided into two groups, i.e. 24 and 48 h (n = 3). A 100 μl solution of AuNPs was intravenously injected into mice and then euthanized at assigned time points. The vital organs (liver, kidney, spleen, heart, and lungs) were removed and initially stored in 10% formalin that was further processed through the paraffin embedding technique for histopathology. The H&E staining technique was used to stain the cell nucleus and cytoplasm differentially. Afterward, the slides were observed under an Olympus fluorescence microscope at 20 X.

2.11. Statistical analysis

The data were initially recorded in MS Excel. Then, the difference in mean was measured by analysis of variance via statistical software SPSS. version 18 (SPSS Inc. Chicago IL). The probability value < 0.05 was considered as statistically significant. All the experiments were performed in triplicate otherwise specified. The data presented are the mean ± standard deviation (SD).

3. Results

3.1. Fabrication and characterization of AuNPs

The AuNPs were biosynthesized by a very facile method of mixing $HAuCl_4$ solution with aged cell culture medium, and a color change of the solution from light yellow to red was observed that indicated the formation of AuNPs (Scheme 1). Then, the TEM, energy dispersive spectroscopy (EDS), X-ray photon spectra, UV–vis spectroscopy, and DLS technique were employed to characterize the obtained nanoparticles and made a comparison with the AuNPs synthesized by the conventional chemosynthesis method as described earlier [26]. As shown in Fig. 1A and B, the biosynthesized AuNPs were monodisperse with an average diameter of 3.6 ± 0.28 nm, smaller than the chemosynthesized AuNPs (9.6 ± 0.067 nm) that were prepared under standard citrate method *in vogue*. The zeta potential of the biosynthesized AuNPs was (−48 mv) almost similar to the chemosynthesized one (−51 mv) (Fig. 1C), suggesting their excellent dispersibility in aqueous media [27]. Moreover, there was no difference in the UV–vis absorbance of the biosynthesized and chemosynthesized AuNPs, i.e. around 540 nm (Fig. 1D). The absorbance peaks of biosynthesized and chemosynthesized AuNPs are according to the earlier reports [26,28].

A HR-TEM image of one typical spherical AuNPs is shown in Fig. 2A and SI1A. An evident lattice fringe indicating a lattice spacing of ca. 0.235 nm, which corresponds to the [111] facets of Au, could be easily observed in a high population in the representative HR-TEM images. Meanwhile, lattice fringes with a lattice spacing of ca. 0.204 nm, corresponding to the [200] planes of Au, could also be detected occasionally in a small fraction. Experimentally, we found that there are no other lattice facets as fringes ascribed. Likewise, the face-centered cubic structure of biosynthesized AuNPs and spots in the single crystal of selected area electron diffraction pattern are indexed and reveal that the particles are single, isolated, and crystalline **(SI1B)**.

The EDS analysis was used to verify the purity and composition of the gold nanoparticles (Fig. 2B). An EDS pattern displays a very high content of Au, which indicates the purity of the nanoparticles. Several other peaks were also observed that could be attributed to the substrate used. Similarly, the XPS was performed to determine the composition, surface chemical state, and surface concentration of the AuNPs. The XPS spectra have proven the presence of a strong gold signal, indicating that substantial low level of impurities. Thus, it confirms the presence of high-purity AuNPs. Coating organic materials may surround the AuNPs, describing for the other peaks attributed to C, N, and O. Two separate peaks located at 84.1 and 88.2 eV are attributed to Au($4f^{5/2}$) and Au($4f^{7/2}$) transitions, respectively (Fig. 2C and D). A positive shift for the Au(4f) peaks in the spectrum was observed for the AuNPs. The obtained peaks were assigned to the spin-orbit splitting component of the Au($4f^{5/2}$ and $4f^{7/2}$) level in metallic gold, whereas the binding energies of 84.1 and 88.2 for the Au(4f) peaks correspond to Au^+ and Au^{3+} respectively, as previously reported [29] and are also in line with reports for biosynthesized AuNPs that utilized intracellular cancer scaffold [11,30].

3.2. Cell type effect on AuNPs biosynthesis

To investigate whether this biosynthesis procedure can be extended to other types of cancer cells, aged cancer cells culture medium from cervical (HeLa), gastric (MGC803), and breast (MCF-7) cancer cells were utilized for biosynthesis of AuNPs. Encouragingly, well-defined AuNPs were obtained from all of the culture medium-aged at 24 h. The HeLa, MGC803, and MCF-7 cancer cells culture media produced AuNPs particle size mean ± standard deviation of 70 ± 44 (range: 21 to164), 31.35 ± 18 (range: 11.7 to 68), and 121 ± 69 (range 37.84–255) nm, respectively (Fig. SI2). The difference in the biosynthesized AuNPs size may be attributed to the cancer cell type and different concentrations of cell biomolecules [31]. The zeta potential of these biosynthesized AuNPs was also comparable to the chemosynthesized AuNPs (Fig. SI3). Moreover, to investigate the difference between cancer and healthy cells, the monocytes (Mp) aged cell culture media was employed to biosynthesize the AuNPs with a size mean of 171 ± 54 (range: 105–256 nm) and had ~ 40% lower yield and larger size as compared with cancer cells culture aged medium (Fig. SI2 & 3). Likewise, the macrophage cell line 24 h aged cell culture media could produce the AuNPs with an average mean size of 177 ± 43 nm, almost the same to monocytes biosynthesized AuNPs

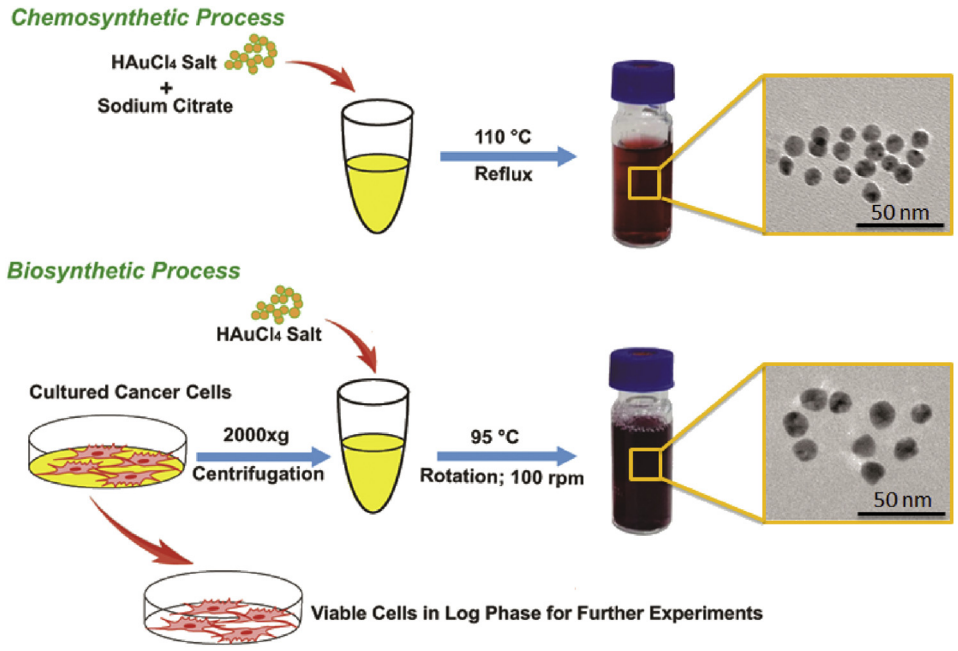

Scheme 1. Gold nanoparticles biosynthesis from the aged cancer cell culture media and its comparison with the chemosynthetic process currently *in vogue*.

(Fig.SI4A, B). Besides, there was a clear absorbance range difference between healthy and cancer cell lines aged medium produced AuNPs (Fig. SI5A).

3.3. Incubation time and confluency effect

It was observed that the aged culture media incubation time and cell number could significantly affect the AuNPs size. We investigated the role of cell number on the AuNPs biosynthesis. The different concentrations (0.5×10^6, 1.0×10^6, 1.5×10^6, 2.0×10^6, 2.5×10^6 and 3.0×10^6 cells in six-well plates) of cancer cells (U87) at 24 h incubation demonstrated that increase in the number of cells had a significant size lowering effect on the biosynthesized AuNPs, i.e. from several hundred to below 10 nm (Fig. 3A). Furthermore, six various types of cell lines were used to confirm the cancer cells' effect on the size of biosynthesized AuNPs, and all cells aged media could significantly lower the AuNPs size

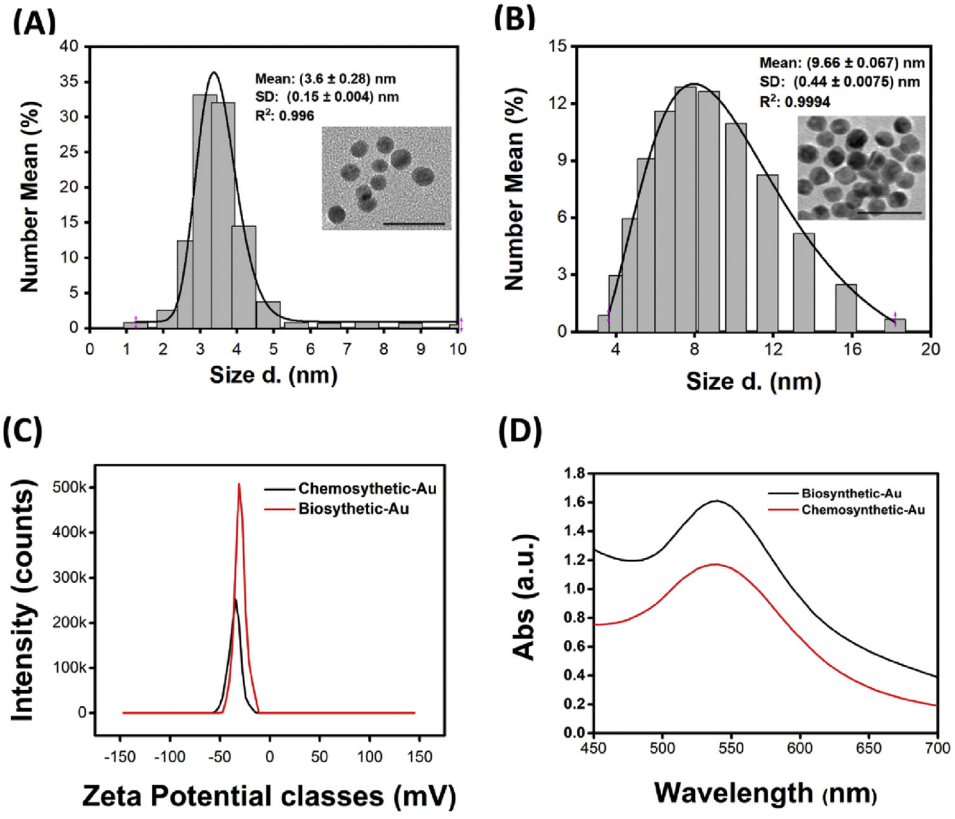

Fig. 1. Characterization and comparison of conventional chemosynthesized AuNPs with a cancer cell (glioblastoma U87 cell line) aged culture media biosynthesized AuNPs. Herein, (A) is the size distribution of biosynthesized and (B) is the chemosynthesized AuNPs (the inset are the TEM micrographs of AuNPs). The scale bar is representing 50 nm sizes. Similarly, (C) and (D) are the absorption and zeta potentials of chemo and biosynthesized AuNPs. AuNPs, Au nanoparticles; TEM, transmission electron microscopy.

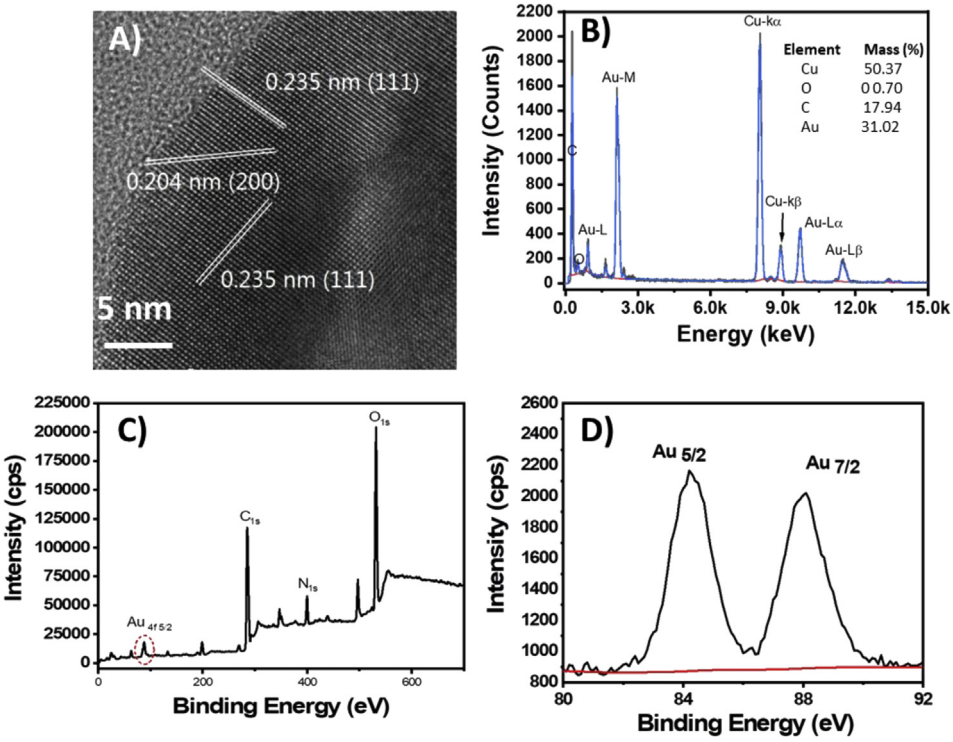

Fig. 2. Characterization of biosynthesized AuNPs from aged cancer cells culture medium. (A) The Fringe spacing for interplanar distance confirming AuNPs fabrication, (B) is the TEM-EDS spectra for Au, whereas (C, D) are the XPS spectra of the Au 4f level of biosynthesized AuNPs from U87 cancer cells. AuNPs, Au nanoparticles; TEM, transmission electron microscopy; XPS, X-ray photoelectron spectroscopy; EDS, energy dispersive spectroscopy.

with an increase in the cell number (Fig. 3B). Meanwhile, the healthy cells (L02) at the same cell concentration had no significant effect on the size lowering of AuNPs (Fig. SI6).

3.4. Serum proteins influence of AuNPs

To investigate the differential factor present in the cancer cells responsible for the AuNPs size control, we in situ spiked the $HAuCl_4$ solution with various factors viz glucose, reduced glutathione (GSH), H_2O_2, genetic material (RNA), FBS with and without protein, DMEM medium, serum proteins, and DMEM supplemented with 10% FBS. Among them, serum proteins, DMEM with and without 10% FBS, were able to biosynthesize AuNPs under standard conditions (Fig. 4A). We further investigated various types of proteins that constitute the cell microenvironment, i.e. serum albumin, cytochrome C, hemoglobin, transferrin, cell culture aged medium isolated proteins at ultracentrifugation (120,000×*g*), and FBS isolated proteins. Surprisingly, the latter three were able to biomineralize the $HAuCL_4$ to AuNPs under the standard conditions. (Fig. 4B, C, D). It was demonstrated that the cancer cell medium could significantly lower the AuNPs size as compared with fresh and healthy cell culture media (Fig. 5A and B). Similarly, when we spiked the same type of media with cancer cell isolated protein (i.e. 150 μg/mL), the size of all biosynthesized AuNPs was lowered, even the fresh DMEM also lowered the AuNPs size (Fig. 5C). These results indicate that cancer cells' soluble factors and proteins both have a strong synergistic effect on the size lowering of the biosynthesized AuNPs.

3.5. Biosynthesized AuNPs BBB traversing ability

The BBB crossing ability of biosynthesized AuNPs was evaluated by the trans-well method *in vitro* and animal studies *in vivo*. Both data confirmed excellent BBB crossing ability of AuNPs. The *in vitro* fluorescence confocal imaging showed higher uptake in U87 cells after BBB crossing by biosynthesized AuNPs (Fig. 6A). Meanwhile, the chemosynthesized AuNPs exhibited significantly ($p < 0.01$) lowered BBB traversing ability, as shown in Fig. 6B and Fig. SI7. Likewise, the animal models showed higher fluorescence in the brain of mice treated with biosynthesized AuNPs at various time intervals, i.e. 01, 12, 24 h (Fig. 6D and E). Meanwhile, the fluorescence intensity of various organs (Fig. 6F) and ICP (Fig. 6G) data both confirmed higher AuNPs uptake in the brain, followed by the liver and kidney.

3.6. Biocompatibility of biosynthesized AuNPs

3.6.1. In vitro

For the cellular uptake of the biosynthesized and chemosynthesized AuNPs, the U87 cells were 24 h incubated with 30 μM AuNPs under standard incubation conditions and bioimaged via a confocal microscope. The cellular uptake and fluorescence (excitation at 488 nm) properties of chemosynthesized and biosynthesized AuNPs had no difference (Fig. SI8A). Also, a comparative MTT assay was performed to check the fibroblast cell viability. The results suggested that at higher doses of 150 and 225 μM, the biosynthesized AuNPs remained less toxic as compared with chemosynthesized ones (Fig. SI8B).

3.6.2. In vivo

For *in vivo* biocompatibility, 100 μl of 10 mg/mL biosynthesized and chemosynthesized AuNPs were injected into the mouse models for 24 and 48 h. The vital organ histopathology indicated the biocompatibility of biosynthesized AuNPs (Fig. SI9). Meanwhile, the fluorescence imaging also showed prolonged accumulation of chemosynthesized AuNPs in vital organs as compared with biosynthesized (Fig. SI10). During histopathology investigations, in the chemosynthesized AuNPs group the lung's broken alveolar epithelium, presence of inflammatory cells in the liver and increased space between glomerulus and bowmen's capsule in the kidney at 48 h

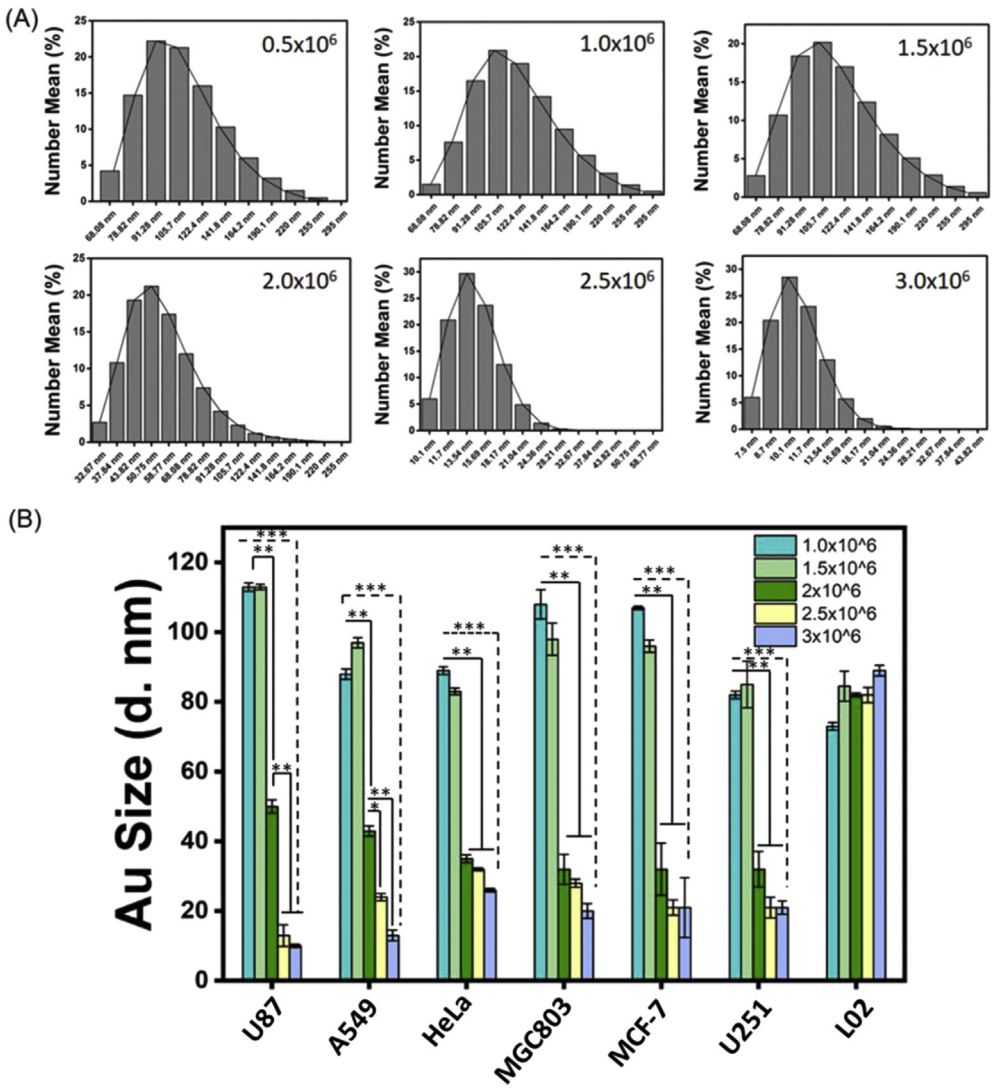

Fig. 3. The cancer cell number effect on the $HAuCl_4$ biomineralization. Herein, (A) is the glioblastoma, i.e. U87 cells and (B) representing various types of cancer and their cell number influencing the size of biosynthesized AuNPs. Here the *, **, and *** are representing probability value at 0.05, 0.01, and 0.001, respectively. AuNPs, Au nanoparticles.

vouch chemosynthesized AuNPs adverse effects that were absent in the biosynthesized AuNPs at the same time interval.

4. Discussion

In the recent few decades, an exponential increase in nanotechnology for biomedical applications have revolutionized the modern therapeutics [32,33]. Nevertheless, nanoscale materials fabrication processes and adverse effects have also brought serious concerns to the biomedical research community. It has been reported that globally around 1300 nanomaterials are produced every year (http://www.nanotechproject.org/); among them, few are environment-friendly because of highly hazardous chemical use during the fabrication process. Therefore, inert and biocompatible materials fabrication is highly desired.

In this study, we observed that the $HAuCl_4$ biomineralization to AuNPs is driven by three main factors, i.e. cell culture medium ingredients, a pool of vital factors from cells, and proteins (mainly transferrin). Because the aged cell culture media is rich in various biofunctional molecules, especially proteins, which interact with the surface of the nanoparticles, and this nanobio interface makes AuNPs amenable for rapid cellular interactions [34]. It was found during the TEM that biosynthesized AuNPs had a protein corona on their surface that makes them highly biocompatible and can easily be uptaken by cells as previously been explained by Sotnikov et al. [35]. Upon interaction with biological fluids, a series of biological molecules confer upon the pristine nanomaterials termed as the corona, and it decides the fate of nanomaterial. Moreover, the reticuloendothelial rapid clearance is one of the significant limitations for the nanoscale materials biomedical applications [36]. Therefore, the protein corona precoated on the nanomaterials may program the fate of nanomaterials. For instance, the transferrin protein corona promotes clathrin-mediated endocytosis [37].

Previously, it was reported that chemosynthesized AuNPs, when interacted with cell culture media, could produce protein corona on its surface, which was attributed to the serum proteins coating [38]. The cystine content of serum protein is considered highly cationic toward the metallic surfaces [39]; likewise, the transferrin is comprised of half-cystine molecules, hence shows affinity to the Au, which is driven by the electrostatic forces on its surface [40,41]. Cox et al. evaluated the protein corona on the presynthesized AuNPs before and after BBB traverse [42]. It was found that protein corona post-traverse was more stable as compared with the pre-BBB traverse. They attributed this corona stability to detachment of specific proteins before BBB traverse that could hamper the nanomedicine traversing, allowed new protein interaction with higher stability post-BBB traverse. Our approach is

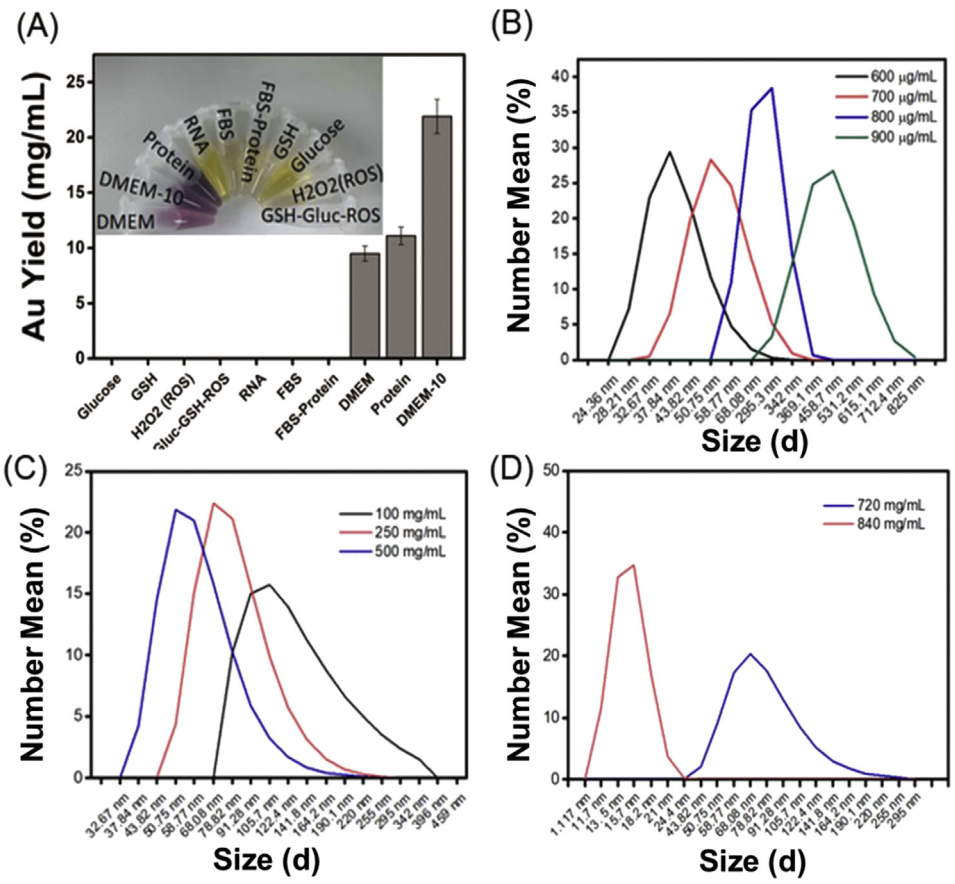

Fig. 4. Neoplastic microenvironment's various biological factors initiating $HAuCl_4$ biomineralization to fabricate AuNPs. Herein, (A) is the cancer cell microenvironment factors changing the color from yellow to reddish is the indication of AuNPs biosynthesis after spiking and their respective yield in mg/mL, (B) is the cancer cell culture aged medium isolated proteins at various concentrations. Similarly, (C) is the biosynthesized AuNPs in the presence of transferrin, whereas (D) is total serum proteins isolated from fetal bovine serum through ultracentrifugation responsible for the AuNPs biosynthesis. (For interpretation of the references to color in this figure legend, the reader is referred to the Web version of this article.) AuNPs, Au nanoparticles.

different from these studies, as we have employed the cell culture media to biosynthesize the AuNPs, and during fabrication, the protein corona was also established on the AuNPs surface. In contrast, they employed the cell culture media for protein corona establishment on the presynthesized AuNPs. Therefore, the protein corona stability may not be inferior to already published data [43–46] that has been evidenced by higher BBB traversing both *in vitro* and *in vivo*.

The cell culture media is comprised of amino acids and peptides, glucose, inorganic salts, growth factors, and hormones rich serum along with pH and osmolality stabilizers [47]. Besides, the high pool of reduced and oxidized glutathione (GSH-GSSG), NAD(P)H, ROS, etc. from cancer cells, and ingredients of culture media also contribute to biomineralization. For instance, the inorganic salts of cell culture media provide ions (e.g. Na^+, K^+, Zn^{2+}, Fe^{2+}), in addition to hydroxyl and carboxyl ions provided by the cancer cells, assist in AuNPs initial seeding (Au^o) that acts as nucleation center catalyzing other ions to biomineralize [48]. Similarly, in analogy to gallic acid that was reported as reducing and stabilizing agent for AuNPs formation [49], in cancer cells, the GSH-GSSG can be a contributing factor for Au biomineralization.

Earlier, protein source from fungi has been reported to form AuNPs [28]. Our results suggest that total serum and cell protein have a direct relationship with AuNPs size. In contrast, transferrin has an inverse relationship with AuNPs size, i.e. higher the concentrations of transferrin lower the particle size. As the transferrin has a crucial role in Fe^{2+} transportation to the cells, therefore higher concentration of transferrin will result in increased Fe^{2+} ions availability to reduce Au [3] to Au^0. The Fe^{2+} reducing role in AuNPs has already been reported [11]. We are of the view that cell protein concentration has a pivotal role in AuNPs formation. However, the additional factors from cancer cells culture media also significantly contribute to the size lowering.

During the healthy and cancer cells aged media comparative effect study on AuNPs, it was revealed that the various cell's microenvironment was size influencing factor, whereby except the cell number and type, all the other conditions were constant. The production of a relatively higher number of GSH-GSSG (i.e. around 10 mM in cancer cells [9]), NAD(P)H,

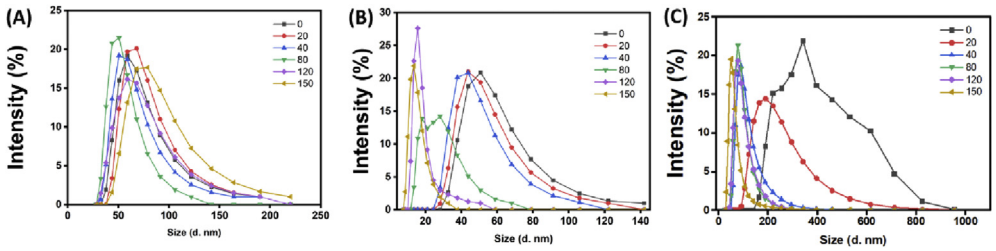

Fig. 5. Cellular factors influencing the size of biosynthesized AuNPs. (A) is the healthy cells (i.e. L02) discarded medium, (B) is the cancer cell line (i.e. U87), and (C) is the fresh cell culture medium (DMEM) spiked with glioblastoma cells culture discarded medium isolated proteins through ultracentrifugation. The 0 to 150 are various proteins concentrations in µg/mL, whereas the medium and $HAuCl_4$ were mixed at 1:1 under described conditions. AuNPs, Au nanoparticles.

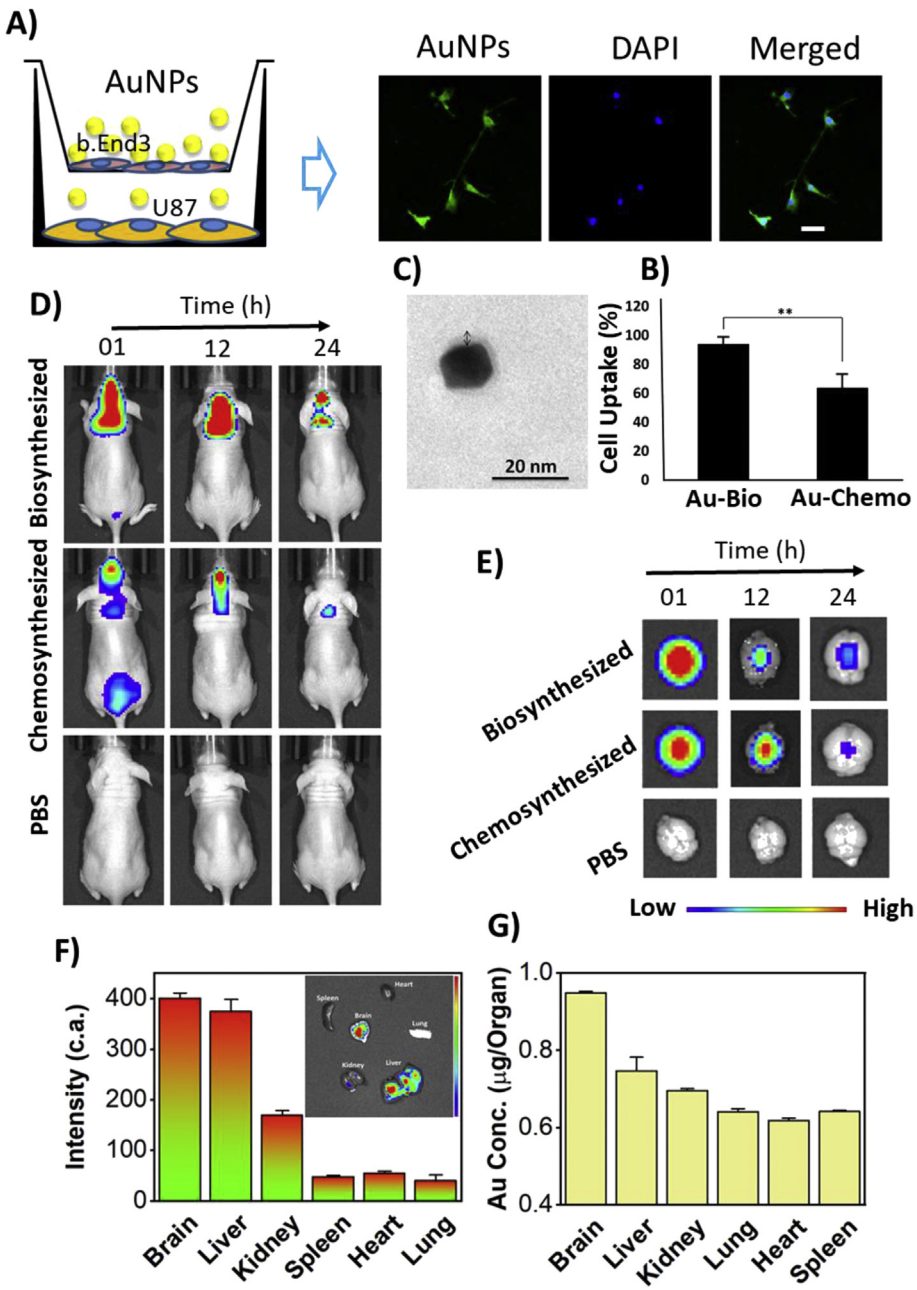

Fig. 6. Biosynthesized AuNPs BBB transversion ability. (A) is the *in vitro trans*-well BBB AuNPs crossing data, showing confocal micrographs of AuNPs after 24 h incubation and their transversion through endothelial cells. The scale bar is 50 μm. (B) is the percent fluorescence intensity of AuNPs crossing BBB and uptaken by the U87 cells. Bio refers to biosynthesized and Chemo to chemosynthesized AuNPs. ** is representing $p < 0.01$. C) is the AuNPs TEM micrograph showing protein corona on their surface, i.e. presented with a double arrowhead, (D) is the *in vivo* BBB crossing ability comparison at various time intervals of chemo and biosynthesized AuNPs, whereas (E) is the brain fluorescence micrographs showing Au accumulation at multiple timepoints. (F) is the fluorescence intensity data of the brain and vital organs after treatment with biosynthesized AuNPs, whereas inset is the brain and vital organs fluorescence micrograph after 24 h treatment. Likewise, (G) is the ICP data of mice models treated with biosynthesized AuNPs, showing higher concertation of AuNPs in the brain flowed by the liver and kidney. The fluorescence of AuNPs was measured at excitation 488 nm and emission at 670 nm. AuNPs, Au nanoparticles; BBB, blood-brain barrier; ICP, inductively coupled plasma.

ROS, etc. in addition to membrane proteins and nucleic acids resulted from rapidly proliferating cancer cells are responsible for size control of the cells. The higher yield of AuNPs is obtained from the aged cancer cell culture medium as compared with a healthy one. The acidic environment favors nucleation and crystal growth, resulting in multifaceted AuNPs formation. This can be attributed to the reduction in $AuCl_4^-$ repulsion force and carboxylic group in the medium at lower pH. Kumari et al. have reported that during biosynthesis of AuNPs from fungi extract, the pH could tune the shape of nanoparticles, and small nanoparticles (<10 nm) with round shape can be obtained [28].

Meanwhile, during the UV–vis spectra analysis, it was observed that biosynthesized AuNPs from various healthy cells had absorbance ranged from 534 to 537 nm. In contrast, different types of cancer cells aged medium biosynthesized AuNPs absorbance had a range from 542 to 547 nm. Meanwhile, no significant difference was observed in the UV–vis spectra of U87 cells aged medium biosynthesized AuNPs at various cell concentrations (Fig. SI5B), which indicates that only cancer cells type, not their number is effecting absorbance of AuNPs.

The earlier studies have demonstrated intracellular gold nanoclusters formation in various types of neoplastic tissues and cultured cancer cells [8,50,51]. The intracellular nanoclusters formation has been observed near the nuclear membrane that is rich in mitochondria and enzymatic pool, especially NO-synthases and NAD(P)H-oxidases [52]. Because the neoplastic microenvironment is hypoxic, this activates hypoxia-inducible factor within cancer cells that, in turn, activates genes, growth-promoting factors, and glycolytic enzymes (i.e. glyoxalase-1). The glyoxalase-1 upon exposure can reduce the $HAuCl_4$ to gold nanoparticles [53]. Indeed, these factors are released into the cell culture media that may account for the biomineralization of $HAuCl_4$ to AuNPs.

The excellent biocompatibility and BBB crossing ability of AuNPs can be attributed to their biogenic nature by utilizing mammalian cells scaffold. The presence of transferrin protein corona on the

AuNPs surface (Fig. 6C) facilitates the BBB traversing via transferrin receptors present only on the brain capillary endothelium [54]. The transferrin receptors allow iron transportation via endogenous circulating transferrin protein to brain milieu. Several studies have used these receptors to successfully deliver the nanoscale materials to the brain milieu across BBB [55–57]. Our study is different from the previous reports because they used cancer cells for biosynthesis, and the biomineralization was driven by the parent cells. In contrast, we have exploited the potential of aged cell culture media containing no cells or tissue.

5. Conclusion

In conclusion, we report the most facile, green, and biocompatible modality for AuNPs synthesis from the aged cell culture medium proteins, especially the transferrin that can tune the AuNPs size up to 2 nm. Furthermore, the biosynthesized AuNPs because of the biological scaffold utilization for fabrication are more biocompatible than chemosynthesized AuNPs. Moreover, the biosynthesized AuNPs have excellent BBB crossing ability because of protein corona on their surface driven by the transferrin receptors on endothelial cells, showing their potential application in brain theranostics. The reported technique is novel and first of its kind (to the best of our knowledge).

Credit author statement

F.U.R. and P.M. have conducted all the experiments, and M.A., J.B., and S.H. performed the physical characterization of nanomaterials and data analysis. F.U.R. and W.H. performed confocal microscopy and animal experiments. F.U.R designed the experiments and discussed the results.

Declaration of competing interest

The authors declare that they have no known competing financial interests or personal relationships that could have appeared to influence the work reported in this paper.

Acknowledgment

The authors acknowledge the China Postdoctoral Foundation.

Appendix A. Supplementary data

Supplementary data to this article can be found online at https://doi.org/10.1016/j.mtbio.2020.100072.

References

[1] S. Nie, et al., Annu. Rev. Biomed. Eng. 9 (2007) 257.
[2] H. Yi, et al., Bone Research 4 (2016) 16050.
[3] F.U. Rehman, Biomed. Lett. 6 (1) (2020) 17.
[4] L. Papadimitriou, et al., Materials Today Bio (2020) 100043.
[5] M.A. Rauf, et al., Biomed. Pharmacother. 116 (2019) 108983.
[6] S. He, et al., Mater. Lett. 61 (18) (2007) 3984.
[7] A. Ahmad, et al., J. Biomed. Nanotechnol. 1 (1) (2005) 47.
[8] F.U. Rehman, et al., Nanomed. Nanotechnol. Biol. Med. 14 (8) (2018) 2619–2631.
[9] F.U. Rehman, et al., J. Mater. Chem. B 6 (41) (2018) 6501.
[10] L. Lai, et al., Langmuir 33 (36) (2017) 9018.
[11] C. Zhao, et al., Small 12 (45) (2016) 6255.
[12] T. Du, et al., Nano Research 10 (2017) 2626.
[13] F.U. Rehman, et al., J. Mater. Chem. B 6 (41) (2018) 6501–6514.
[14] S. Shaikh, et al., ACS Appl. Mater. Interfaces 10 (31) (2018) 26056.
[15] S. Tortorella, T. C Karagiannis, Curr. Drug Deliv. 11 (4) (2014) 427.
[16] A. Heuer-Jungemann, et al., Chem. Rev. 119 (8) (2019) 4819.
[17] E.R. Evans, et al., Mater. Today 21 (6) (2018) 673.
[18] M.D. Sweeney, et al., Nat. Rev. Neurol. 14 (3) (2018) 133.
[19] N.J. Abbott, et al., Nat. Rev. Neurosci. 7 (1) (2006) 41.
[20] M. Srikanth, J.A. Kessler, Nat. Rev. Neurol. 8 (6) (2012) 307.
[21] A. Qambrani, Biomed. Lett. 5 (1) (2019) 1.
[22] F. Rehman, et al., Biomaterials science 4 (1) (2016) 40.
[23] S. Ding, et al., Mater. Today 37 (2020) 112–125.
[24] R. Gonçalves, D.M. Mosser, Curr. Protoc. Im. 111 (14) (2015) 1, 1.
[25] G. Lisignoll, et al., Connect. Tissue Res. 42 (1) (2001) 49.
[26] J. Kimling, et al., J. Phys. Chem. B 110 (32) (2006) 15700.
[27] J.D. Clogston, A.K. Patri, Zeta potential measurement, in: Characterization of Nanoparticles Intended for Drug Delivery, Springer, 2011, p. 63.
[28] M. Kumari, et al., Sci. Rep. 6 (2016) 27575.
[29] D.A. Bulushev, et al., J. Catal. 224 (1) (2004) 8.
[30] F.U. Rehman, et al., Nanomed. Nanotechnol. Biol. Med. 14 (8) (2018) 2619.
[31] R.M. Day, Y.J. Suzuki, Dose-response 3 (3) (2005) 425.
[32] M.K.M. Younas Iqbal, Jianli Wang, Chao Wang, Uzair majeed, pir muhammad, fawad ur rehman, imtiaz ahmad, Biomed. Lett. 6 (1) (2020) 60.
[33] H. Su, et al., Materials Today Bio (2019) 100033.
[34] G. Maiorano, et al., ACS Nano 4 (12) (2010) 7481.
[35] D.V. Sotnikov, et al., Colloids Surf. B Biointerfaces 173 (2019) 557.
[36] A.V. Singh, et al., ACS Nano 11 (10) (2017) 9759.
[37] M.S. Boyles, et al., J. Nanobiotechnol. 13 (1) (2015) 84.
[38] E. Casals, et al., ACS Nano 4 (7) (2010) 3623.
[39] B.P. Rosen, JBIC Journal of Biological Inorganic Chemistry 1 (4) (1996) 273.
[40] M.C.M. Chung, Biochem. Educ. 12 (4) (1984) 146.
[41] M.-M. Yin, et al., Langmuir 33 (21) (2017) 5108.
[42] A. Cox, et al., ACS Nano 12 (7) (2018) 7292.
[43] Y.T. Ho, et al., Bioconjugate Chem. 29 (11) (2018) 3923.
[44] B.D. Johnston, et al., Adv. Funct. Mater. 27 (42) (2017) 1701956.
[45] A. Lesniak, et al., Biomaterials 31 (36) (2010) 9511.
[46] J. Piella, et al., Bioconjugate Chem. 28 (1) (2017) 88.
[47] M. Arora, Mater methods 3 (175) (2013) 24.
[48] N. Basavegowda, et al., Ind. Crop. Prod. 52 (2014) 745.
[49] N.K.R. Bogireddy, et al., J. Mol. Liq. 211 (2015) 868.
[50] Anshup, et al., Langmuir 21 (25) (2005) 11562.
[51] J. Wang, et al., Sci. Rep. 3 (2013) 1157.
[52] C. Amatore, et al., Chem. Rev. 108 (7) (2008) 2585.
[53] H. Sakamoto, et al., Clin. Canc. Res. 7 (8) (2001) 2513.
[54] W.A. Jefferies, et al., Nature 312 (5990) (1984) 162.
[55] S. Tortorella, T.C. Karagiannis, J. Membr. Biol. 247 (4) (2014) 291.
[56] E.A. Nance, et al., Sci. Transl. Med. 4 (149) (2012) 149ra119.
[57] K.B. Johnsen, T. Moos, J. Contr. Release 222 (2016) 32.